IOPscience iopscience.iop.org

Home Search Collections Journals About Contact us My IOPscience

Reactive gas pulsing sputtering process, a promising technique to elaborate silicon oxynitride multilayer nanometric antireflective coatings

This content has been downloaded from IOPscience. Please scroll down to see the full text.

2017 J. Phys. D: Appl. Phys. 50 015306

(http://iopscience.iop.org/0022-3727/50/1/015306)

View the table of contents for this issue, or go to the journal homepage for more

Download details:

IP Address: 193.54.50.250
This content was downloaded on 24/11/2016 at 13:49

Please note that terms and conditions apply.

IOP Publishing
Journal of Physics D: Applied Physics
J. Phys. D: Appl. Phys. **50** (2017) 015306 (9pp)
doi:10.1088/1361-6463/50/1/015306

Reactive gas pulsing sputtering process, a promising technique to elaborate silicon oxynitride multilayer nanometric antireflective coatings

A Farhaoui[1,2], A Bousquet[1,2], R Smaali[3,4], A Moreau[3,4], E Centeno[3,4], J Cellier[1,2], C Bernard[5], R Rapegno[5], F Réveret[3,4] and E Tomasella[1,2]

[1] Institut de Chimie de Clermont-Ferrand, Université Clermont Auvergne, Université Blaise Pascal, BP 10448, F-63000 Clermont-Ferrand, France
[2] CNRS, UMR 6296, ICCF, F-63178 Aubiere, France
[3] Institut Pascal, Université Clermont Auvergne, Université Blaise Pascal, BP 10448, F-63000 Clermont-Ferrand, France
[4] CNRS, UMR 6602, IP, F-63178 Aubière, France
[5] Institut de Physique Nucléaire de Lyon, CNRS/IN2P3, UMR 5822, Université Claude Bernard Lyon 1, Université de Lyon, 4 rue Enrico Fermi, F-69622 Villeurbanne cedex, France

E-mail: Angelique.Bousquet@univ-bpclermont.fr

Received 29 January 2016, revised 29 August 2016
Accepted for publication 13 September 2016
Published 24 November 2016

Abstract

The oxynitride materials present a high versatility, which enables their properties to be controlled by tuning their elemental composition. This is the case for silicon oxynitrides used for multilayer antireflective coatings (ARCs), where several thin films with various refractive indexes are needed. Different techniques allow for the modification of the thin film composition. In this paper, we investigate the reactive gas pulsing sputtering process to easily tune the thin film composition, from an oxide to a nitride, by controlling the averaged oxygen flow rate, without reducing the deposition rate, compared to a conventional reactive process (CP). We then demonstrated that the refractive indexes of films deposited by this pulsing process (PP) can be varied in the same range compared to films obtained by CP (from 1.83 to 1.45 at 1.95 eV), whereas their extinction coefficients remain low. Finally, the multilayer ARC has been simulated and optimized by a genetic algorithm for wavelength at 600 nm and for the silicon substrate. Various optimized multilayer (mono-, bi- and tri-layers) structures have been deposited by the PP technique and characterized. They are presented in good agreement with the simulated reflectivity. Hence, the PP allows for an easy depositing tri-layer system with a reasonable deposition rate and low reflectivity (8.1% averaged on 400–750 nm visible light range).

Keywords: oxynitride, reactive sputtering, antireflective coating, ellipsometry, FTIR, optical simulation

(Some figures may appear in colour only in the online journal)

1. Introduction

Over the last few decades, oxynitride materials have been extensively studied as potential candidates to tune mechanical, optical or electrical properties between oxide and nitride ones [1–3]. Among them, silicon oxynitrides present a great interest for numerous applications, such as an intermediate dielectric constant for microelectronic [4] or a diffusion barrier for boron, phosphor [5] and also for gas [6, 7]. More recently, they are increasingly used as antireflective coatings and passivation layers to improve efficiency of a solar cell [8–10]. In this domain, a recent study has

© 2016 IOP Publishing Ltd Printed in the UK

for instance shown that multi-layered ARCs using SiO_xN_y give better transmission coefficients than single layered silicon nitride, and therefore they increase the penetration of photons into the solar cell [11]. These silicon oxynitrides are commonly prepared by low-pressure plasma enhanced chemical vapor deposition (PECVD) [8–10]. However, recently, the sputtering process has started to be used in the photovoltaic industries thanks to its several advantages; the process avoids using toxic gases as silane is used as the silicon source, and is of its low cost and high versatility in the deposition of film composition.

The silicon oxynitride deposition from the silicon target sputtering in the $Ar/O_2/N_2$ atmosphere was shown to be possible [12, 13]. However, the reactive sputtering process, especially with two reactive gases, is known to be very difficult to control. Indeed, target poisoning by reactive gas induces a memory effect, which leads to a nonlinear process behavior. This phenomenon is even more complex with two reactive gases because of the competitive reactions between both gases [14–16]. Different techniques can be used to overcome this problem, for instance, a process mapping [16] or a feedback control of reactive gas partial pressure [17]. Another technique was proposed by Aronson *et al*, which consists of pulses to the reactive gas flow rate to switch between the elemental sputtering mode and the compound sputtering one [18]. This technique is called the reactive gas pulsing process (RGPP). It was successfully used to deposit titanium, iron or silicon oxynitride films [2, 19, 20] by firstlyusing a rectangular shape for pulsed flow rate. Later, this technique reached an even better control by using an exponential shape of pulsed flow rate [21].

The present paper aims to use the RGPP for silicon oxynitrides film deposition with a fine tune of elemental composition in order to control their optical properties, especially their refractive indexes. Having materials with a controlled refractive index in a large range, allow us to synthesize antireflective multilayer coatings for a silicon wafer. Our goal is to grow this multilayer system by only changing the pulsed gas flow parameters during silicon target sputtering, contrary to a system where different targets are sputtered to obtain different materials with different refractive indexes, for instance in bilayer of MgF_2–Al_2O_3 or trilayer of MgF_2–ZrO_2–CeF_3 [22]. Furthermore, we aim to obtain this antireflective system not only for normal incident light but also for a large range of incident angles.

In this paper, we will firstly check, as already demonstrated in other papers [20, 21], that the RGPP technique allows us to deposit silicon oxynitride films with a controlled elemental composition. The deposition rates and film structures will also be studied. After that, the optical properties of these films will be more deeply investigated. Finally, an antireflective multilayer system will be simulated, optimized and realized thanks to the RGPP technique.

2. Experimental details

2.1. SiO_xN_y thin film deposition

Silicon oxynitride films were deposited by radiofrequency reactive magnetron sputtering. A pure Silicon target (99.99% and 100 mm in diameter) is placed at 95 mm from the substrate and sputtered in an $Ar/O_2/N_2$ atmosphere. Before the deposition, the sputtering chamber was evacuated to 10^{-5} Pa and then the silicon target was sputtered for 30 min at 250 W in a pure argon atmosphere at 1 Pa to clean up the surface. Then, the gas mixture was introduced for 2 min in order to prepare the target for the reactive conditions. The deposition was then started by removing the shutter in front of the substrate. The Ar, N_2 and O_2 gas flow rates, Φ_{Ar}, Φ_{N_2} and Φ_{O_2} respectively, are controlled by mass flowmeters. For the study, the Ar flow rate was fixed at 7.8 sccm. The radiofrequency power was fixed at 250 W. The total gas pressure was 1 Pa. The substratewas neither biased nor heated. The deposition time was modified to obtain 200 nm thin films for monolayer material characterization or a lower thickness for multilayer elaboration.

Two sets of samples were deposited with conventional (CP) and pulsed processes (PP). The CP referred to a continuous flow rates injection during the film deposition. The oxynitride films were obtained by changing both the O_2 and the N_2 flow rates. In order to keep constant the total pressure, we fixed the total reactive flow rate, $\Phi_{O_2+N_2}$, and we varied the O_2 one in the total reactive flow rate ratio, R_F, from 0 (Ar/N_2 atmosphere) to 1 (Ar/O_2 atmosphere), where R_F is defined by:

$$R_F = \frac{\Phi_{O_2}}{\Phi_{O_2} + \Phi_{N_2}}. \tag{1}$$

In this conventional process mode, we also deposited 3 films illustrating the deposition in an elemental sputtering mode, when the target is pure silicon, and in the compound sputtering mode, where the target was covered by an oxide and by a nitride. For the first sample, only Ar ($\Phi_{Ar} = 7.8$ sccm) was injected, whereas both the other samples were deposited with Ar/N_2 ($\Phi_{Ar} = 7.8$ sccm and $\Phi_{N_2} = 3.0$ sccm) and Ar/O_2 ($\Phi_{Ar} = 7.8$ sccm and $\Phi_{O_2} = 2.2$ sccm) mixtures, respectively.

In PP, Ar and N_2 gases were introduced continuously at constant mass flow rates (7.8 and 1.4 sccm for Ar and N_2 respectively), whereas O_2 was periodically supplied using a rectangular pulsed flow rate, from 0 sccm during the off-time, T_{off}, to a maximum flow rate, $\Phi_{max}(O_2)$, of 0.4 or 0.8 sccm during the on-time, T_{on}. The period, T, was fixed at 20 or 40 s and the duty cyle (DC = T_{on}/T) was varied from 0.1 to 0.9. From these pulse conditions ($\Phi_{max}(O_2)$, T and DC), the average injected O_2 flow rate, $\langle\Phi_{O_2}\rangle$, was defined following this equation:

$$\langle\Phi_{O_2}\rangle = \Phi_{max}(O_2) \cdot \text{DC}. \tag{2}$$

2.2. SiO_xN_y monolayer characterization

The film elemental composition was determined by Rutherford backscattering spectrometry (RBS) using 2 MeV apha particles and 50 nA current intensity. A charge of 40 μC was collected at a detection angle of 172°. Since carbon appears at lower energy than silicon, oxygen and nitrogen, the films were deposited on a

vitreous carbon substrate in order to avoid overlapping between the substrate and film elements. The experimental spectra were simulated using the SIMNRA program [23].

A qualitative bond analysis was performed employing Fourier transformed infrared spectroscopy (FTIR) for absorption measurements in a transmission mode in the range of 400–4000 cm^{-1}, with a resolution of 4 cm^{-1} and 250 scans per spectrum. To limit the infrared light intensity loss, films were deposited on a double side polished intrinsic silicon wafer.

The optical properties of monolayers deposited on silicon substrates were analyzed by spectroscopic ellipsometry in a range of 0.59 to 4.79 eV at a 70° fixed incident angle. The measurements were then simulated with a 'New Amorphous' model. In this model, the dispersion formula, which was derived from the Forouhi-Bloomer formulation, was established to give a Lorentzian shape to the expression of the extinction coefficient and the refractive index, and then this was better for the inter-band absorption [24–26]. In this model, the extinction coefficient and the refractive index are described by the following equations:

$$k(\omega) = \begin{cases} \dfrac{f_j \cdot (\omega - \omega_g)^2}{(\omega - \omega_j)^2 + \Gamma_j^2}; & \text{for } \omega > \omega_g \\ 0; & \text{for } \omega < \omega_g \end{cases} \quad \text{and}$$

$$n(\omega) = n_\infty + \frac{B \cdot (\omega - \omega_j) + C}{(\omega - \omega_j)^2 + \Gamma_j^2},$$

$$\text{where} \begin{cases} B_j = \frac{f_j}{\Gamma_j} \cdot (\Gamma_j^2 - (\omega_j - \omega_g)^2) \\ C_j = 2 \cdot f_j \cdot \Gamma_j \cdot (\omega_j - \omega_g) \end{cases}.$$

In this model, f_j is related to the strength (and so, to the amplitude) of the extinction coefficient peak,

Γ_i is the broadening term of the peak absorption,
ω_i is the light pulsation, at which the extinction coefficient is the maximum,
ω_g is the pulsation corresponding to the band gap energy.

This model is particularly consistent for amorphous materials, which present an absorption in the visible or UV range and was already used to simulate ellipsometric measurements of silicon oxynitride thin films [8].

The optical bandgap was determined from UV–Visible spectroscopy performed with a double beam Perkin Elmer spectrometer in the 200–1100 nm range for films deposited on quartz substrates.

2.3. Multilayer antireflective optical properties simulation and characterization

Among the several gradual index functions (linear, quintic, Gaussian, etc) [27], we chose a linear graded refractive index profile. Ideally the spatial index variation is continuous and varies adiabatically from the lower to the higher optical indices of the targeted materials. This strategy demands a thick ARC and imposes important process constraints to realize the refractive index close to 1 at the air interface. Here, we focus on unmatched refractive index gradients which range from $n_{min} = 1.53$ to $n_{max} = 1.80$, which are boundary values imposed by the available fabrication process conditions. This approach allows us to produce thin ARCs presenting nano-gradients of sub-wavelength spatial variations. Here, the ARCs are backed by the c-Si substrate. The linear gradient is spatially discretized by a step function consisting of a stack of p-layers of equal thicknesses h and refractive indices n_q:

$$\text{Linear profile}: n_q = n_{min} + (n_{max} - n_{min}) \cdot \frac{q-1}{p-1} \quad (3)$$

where q is an integer that varies between 1 and $p-1$. The ARCs are optically optimized according to the number of the layers, p, and to the thickness h to reduce the system's reflectance averaged over wavelengths between 300 nm to 750 nm and for incident angle ranging from 0° to 80°. The refractive indices of the p-layers were chosen for thosethat obtained the wavelength 600 nm since the optical dispersion of SiO_xN_y materials can be neglected for visible frequencies. However, the optical properties of the c-Si substrate were taken into account in the calculations by integrating spectroscopic ellipsometry measurements retrieved in the spectral domain. These electromagnetic simulations are obtained with a homemade code based on a rigorous S-matrix method [28].

To compare with simulation results, the realized multilayer ARCs are characterized by reflectivity measurements. The structures are deposited on a double side polished silicon wafer. Then, measurements are performed at room temperature under normal incidence. A xenon lamp is used as a source light to illuminate the sample. The reflected signal is directed on the slits entrance of a 64 cm focal length monochromator. The optical signal is detected by a CCD camera for the 230–750 nm range, and a germanium detector cooled at liquid nitrogen temperature is used with a lock in amplification for larger wavelengths. Then the recorded signal is normalized with a measurement performed on a standard aluminum mirror.

3. Results and comments

3.1. Composition and deposition rate

The elemental composition is determined by RBS for both film sets deposited with CP and PP. These elemental contents are determined at ±1 at.% due to the RBS measurements incertitude [15]. On the one hand, figure 1(a) presents the Si, O and N contents (in atomic percent, at.%) for films deposited in the continuous process as a function of R_F. We remark that the silicon content is almost constant around 35 at.%, whereas the O and N contents vary in a larger range: from 28 to 63 and from 0.1 to 34 at.% respectively. The film composition can then be characterized by O/(O + N) content ratio, which is plotted in figure 1(b) for films deposited in the CP and PP modes. This ratio changes from 0.34 to 0.94 with $\langle \Phi_{O_2} \rangle$ in PP, and from 0.45 to 1.00 with R_F in CP. This

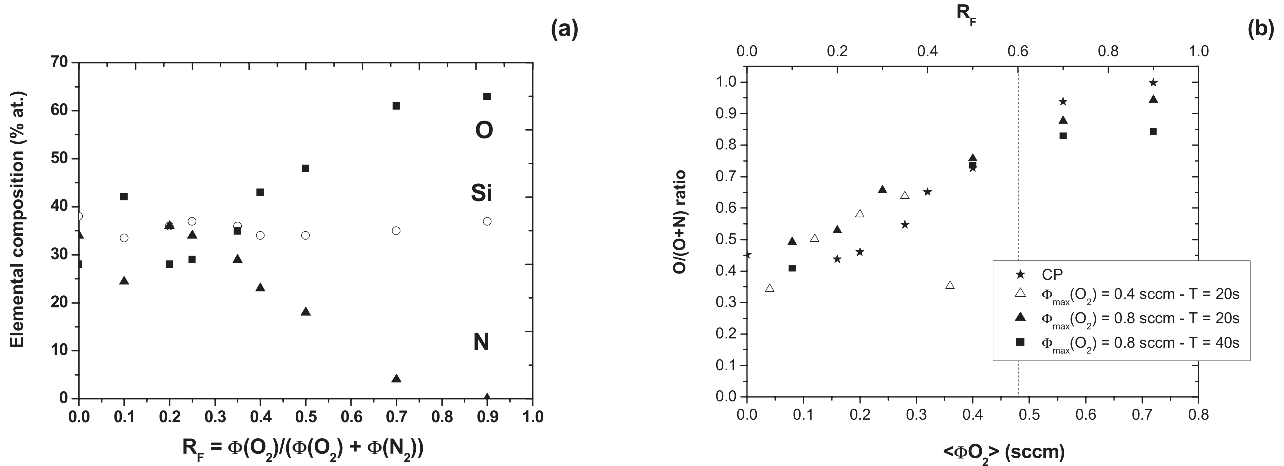

Figure 1. (a) Elemental composition of films deposited in the continuous process and (b) O/(O + N) ratio for films deposited in the continuous (star) and in the pulsed process with different periods and maximum O_2 flow rates.

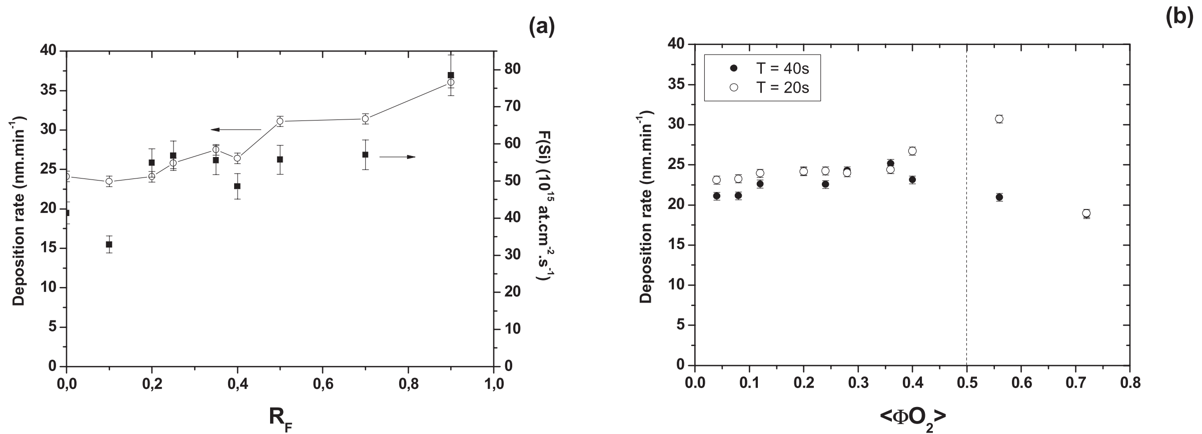

Figure 2. (a) Deposition rates (open) and incorporated silicon flux (full) calculated in CP and, (b) deposition rates in PP for both periods $T = 20$ (open) and 40 s (full).

figure then highlights $\langle \Phi_{O_2} \rangle$ is the main parameter that controls the film composition in PP. For $\langle \Phi_{O_2} \rangle \leqslant 0.4$ sccm, the deposited films are oxynitrides with a linearly increasing O/(O + N) ratio, whereas for $\langle \Phi_{O_2} \rangle \geqslant 0.55$ sccm, the film elemental composition is close to the silicon oxide one (O/(O + N) ratio > 0.8). In the first region ($\langle \Phi(O_2) \rangle > \leqslant$ 0.4 sccm or $R_F \leqslant 0.45$), the films deposited with $T = 20$ s in the PP mode present higher O/(O + N) ratios than those obtained in the CP mode, without being majorly affected by $\Phi_{max}(O_2)$. Indeed, reducing $\Phi_{max}(O_2)$ from 0.8 to 0.4 sccm allows the injection of fine amounts of $\langle \Phi_{O_2} \rangle$ and then reaching smaller modification in oxynitride composition. However, for $\Phi_{max}(O_2) = 0.4$ sccm and DC = 0.9, the O/(O + N) ratio decreases, which could be due to the nature of a different target surface for longer on-time in this condition.

In the second region ($\langle \Phi(O_2) \rangle > 0.5$ sccm or $R_F > 0.6$), the higher O/(O + N) ratios are reached in the CP mode than in PP mode. Moreover, the O/(O + N) ratio for $T = 20$ s (full triangle) is higher than for $T = 40$ s (full square). This second minor effect on film composition could again be due to the influence of target oxidizing and nitriding speeds depending on T_{on} and T_{off} pulse times. This difference in speed was already studied in the reactive gas pulsed sputtering process [20]. However, further study inplasma kinetics is needed for a better understanding. Nevertheless, we can emphasize the interest of the pulsed process to adjust finely the injected O_2 flow rate to control the O and N contents in SiO_xN_y films.

From thicknesses determined by ellipsometry measurements, we calculate the film deposition rates. The figure 2(a) presents values obtained with CP. The growth rates increase slightly from 25 to 35 nm min^{-1} with R_F. These values are close to the ones we classically observed in silicon reactive radiofrequency sputtering [12]. Because of the deposition of additional samples in CP, which correspond to different sputtering modes, we may also notice that these rates are lower than those for the silicon-rich film (at 40 nm min^{-1}) but higher than the values when sputtering an oxidized or a nitrided target, respectively at 8 and 12 nm min^{-1}. This indicates that the deposition does not occur in a compound sputtering mode but in a transition one. For the PP, the deposition rates are plotted in figure 2(b) as a function of $\langle \Phi_{O_2} \rangle$. For $\langle \Phi_{O_2} \rangle \leqslant 0.4$ sccm, the deposition rates are slowly increasing from 20 to 25 nm min^{-1}. For $\langle \Phi_{O_2} \rangle \geqslant 0.55$ sccm, the deposition rates depend on the pulse period: they stay around 20 nm min^{-1} for $T = 40$ s and present a maximum for $T = 20$ s. Overall, all these values are slightly lower than those obtained in CP,

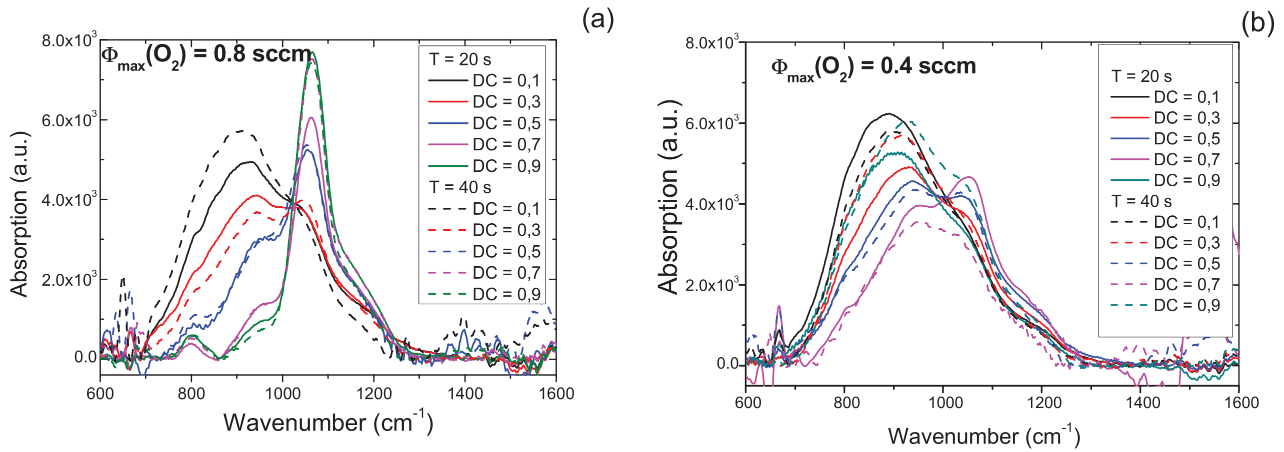

Figure 3. IR spectra for films deposited in PP with various duty cycles, for $T = 20$ s (full line) and $T = 40$ s (dash line), for (a) $\Phi_{max}(O_2) = 0.8$ sccm and (b) $\Phi_{max}(O_2) = 0.4$ sccm.

but they are clearly higher than those observed in the compound sputtering mode. We may consider that the target is not completely poisoned in these conditions, but in the transition mode. Again, the pulse period seems to be a second order influencing parameter. Indeed, deposition rates are slightly higher for shorter pulse period. Since the films deposited with $T = 20$ s are a little bit richer in oxygen, the this is consistent with the small increase of deposition rate with a higher $\langle \Phi_{O_2} \rangle$.

To better understand the growth rate variation, we determine the silicon flux incorporated into the film per time and area unit. It is well known that the poisoned target has a reduced sputtering yield which leads to lower deposition rate [29]. Because of the RBS measurements, the total number of atoms number by area unit, N_{total}, can be known and converted to the silicon flux incorporated into the film per area and time unit, F(Si), using the following equation:

$$F(\mathrm{Si}) = \frac{N_{total} \cdot \%\mathrm{Si}}{t_{deposition}}, \quad (4)$$

where N_{total}: is the total number of atoms incorporated into the film by area unit,

%Si: is the silicon content,
$t_{deposition}$: is the deposition time.

This silicon flux F(Si) is added to figure 2(a) and presents the same evolution than the deposition rate in CP. Indeed, a slight increase of F(Si) for higher R_F explains the slight increase of the deposition rate. This rise could be due to a difference of the target's partial coverage by an oxide and/or a nitride, which influences the total sputtered silicon flux from the target, and/or due to an ion bombarding flux modification with the atmospheric change [14]. In PP, F(Si) is ranging from around 4 – 5 10^{16} at.cm^{-2} min^{-1}. These values of incoming silicon fluxes are relatively close to the one observed in CP (6–8 $\cdot$ 10^{16} at.cm^{-2} min^{-1}), which explains why the deposition rates in PP remain a little bit lower than those in CP. This is also coherent with the sputtering of the target in the elemental or the transition mode, but notwith the compound sputtering mode.

In the literature, similar or larger composition ranges can be reached: O/(O + N) from 0.31–0.95 and 0.15–0.99 for FeO_xN_y and SiO_xN_y respectively in [19, 20], but this is often detrimental to the growth rate: which decreases from 20 to 5 nm min^{-1} or stays around 5–6 nm min^{-1} for FeO_xN_y and SiO_xN_y respectively in [21, 22]. Finally, in the present paper, we confirm that by using the reactive gas pulsing technique, it was possible to deposit films with a relatively large composition variation, depending on pulse parameters, without losing in the deposition speed.

However, the elemental composition determined from RBS measurements is a global composition. So for a better understanding of the films structure, the FTIR measurements have been performed.

3.2. Film structure

The figures 3(a) and (b) show the IR spectra for $\Phi_{max}(O_2) = 0.8$ and 0.4 sccm respectively, focused on the molecular bonding vibrations zone of the Si bonds in the 600–1600 cm^{-1} region. These spectra have been normalized by film thickness in order to plot the absorption. In this region, we may observe the absorption bonds of oxide with Si–O and Si–O–Si bonds (around 1050–1070 and 1100–1250 cm^{-1} respectively), nitride with Si–N (around 790–890 and 960–970 cm^{-1}) and oxynitride with O–Si–N bond (around 850–1000 and at 1100 cm^{-1}) [30, 31]. For $\Phi_{max}(O_2) = 0.8$ sccm, the peak maximum ω_0 shifts towards higher wavenumbers, when the duty cycle increases. For $\Phi_{max}(O_2) = 0.4$ sccm, this shift to a higher wavenumber is again observed when the DC rises to 0.7. However for DC = 0.9, a more important nitride contribution is observed. This unexpected behavior could be due to a specific interaction between both the reactive gases for a long O_2 injection time, but it is also in agreement with the low O/(O + N) ratio observed in figure 1(b). Further studies on the process of the kinetics are needed to explain this point.

The peak maximum ω_0 shifts is seen more clearly in figure 4 as a function of the film composition ratio, demonstrating that it is linked to the film's nature. Hence, for O/(O + N) $\leqslant 0.6$, the ω_0, increase from 891 to 943 cm^{-1} corresponds to the major bonding variation from nitride to oxynitride. For O/(O + N) $\geqslant 0.7$, ω_0 rises to values higher than 1050 cm^{-1}, indicating there is mainly oxide bonding present.

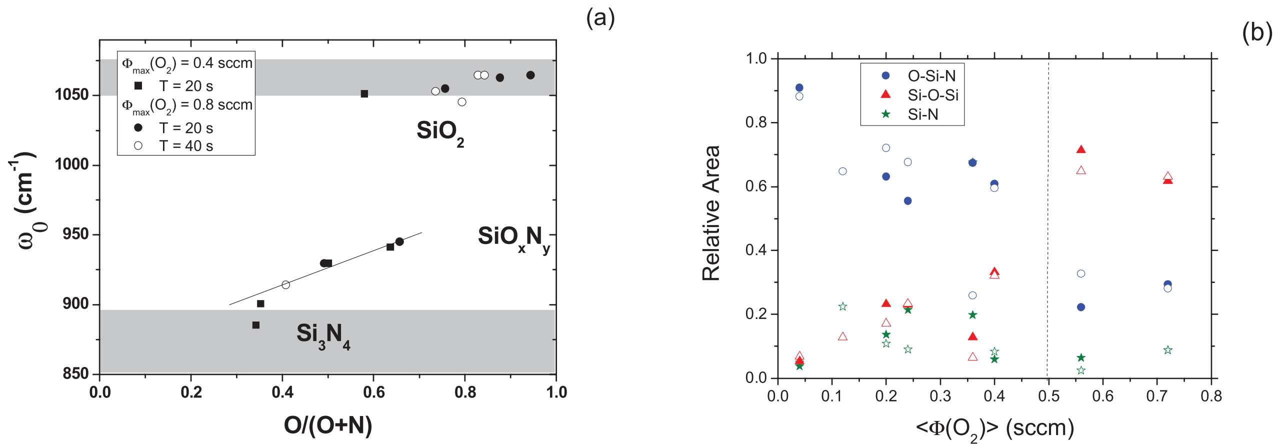

Figure 4. (a) Position of $\omega_{0\,max}$ in IR spectra, and (b) the relative area of three contributions depending on pulsed conditions: $T = 20$ s (open symbols) and $T = 40$ s (full symbols).

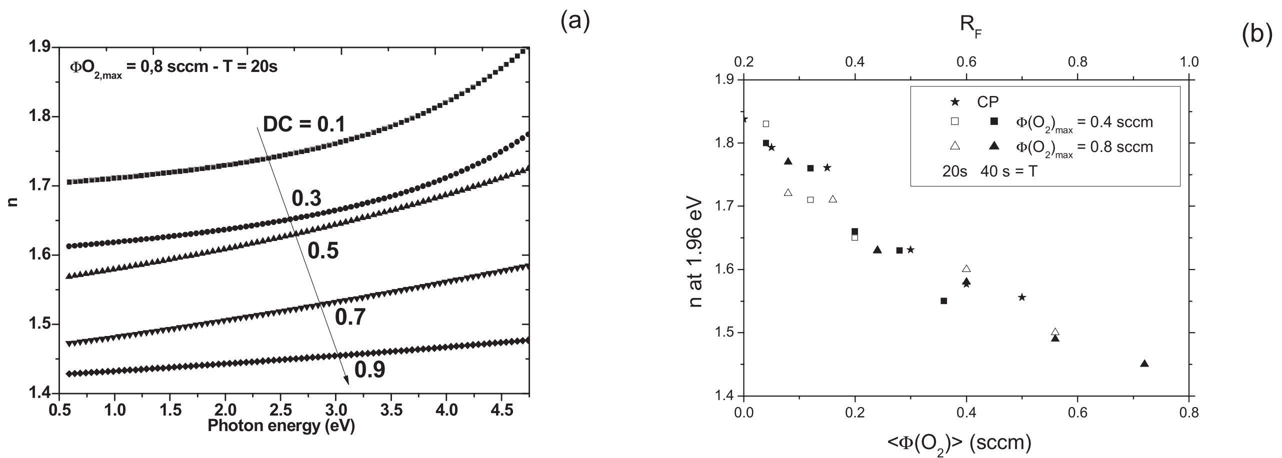

Figure 5. (a) Refractive index as a function of wavelength for $\Phi_{max}(O_2) = 0.8$ sccm, $T = 20$ and various DC, and (b) the refractive index at 1.96 eV as a function of R_F (top axis) and $\langle \Phi_{O_2} \rangle$ (bottom axis) for films deposited in CP and PP respectively.

To go further and check the influence of both $\langle \Phi_{O_2} \rangle$ and the pulse period, all the absorption spectra were decomposed into Gaussian contributions corresponding to the different bonding types, previously reported. The relative contributions of different bonds are plotted in figure 4(b) as a function of $\langle \Phi_{O_2} \rangle$ for $T = 20$ and 40 s. These relative contributions correspond to the contribution of a specific bond peak to the total absorption band. Since the IR absorption peak area depends not only on the bond density, but also on the oscillator strength, we need to pay attention with this plot as the higher relative area does not necessary mean higher bonding content in the film. However, we might observe their qualitative evolution. For $\langle \Phi_{O_2} \rangle \leqslant 0.4$ sccm, the O–Si–N contribution decreases, whereas the oxide bond contribution increases and the Si–N bond contribution stay low. This is in agreement with the ω_0 evolution, indicating oxynitride films. For $\langle \Phi_{O_2} \rangle \geqslant 0.55$ sccm, the oxide bond contribution increases, whereas O–Si–N and Si–N are lower. Again, this is consistent with the ω_0 position around 1050 cm^{-1} and O/(O + N) content > 0.8, corresponding to a film composition close to silicon oxide. Finally, tuning $\langle \Phi_{O_2} \rangle$, thanks to the chosen pulse parameters, controls not only the global atomic concentration in O and N but also the element bonded to silicon.

3.3. Optical properties

After succeeding to finally vary the composition of the SiO_xN_y films, we performed spectroscopic ellipsometry analysis to study their optical properties. The figure 5(a) presents the refractive index in the studied energy range for films deposited with the PP for $\Phi_{max}(O_2) = 0.8$ sccm, $T = 20$ s and for various DC. All of the films' refractive indices have the same evolution with their wavelengths; they only shift to lower n values for the higher DC. The figure 5(b) summarizes the refractive index values at 1.95 eV for films deposited with the PP as a function of $\langle \Phi_{O_2} \rangle$. The $\langle \Phi_{O_2} \rangle$ was shown previously to control the films' elemental composition, and here we can obviously notice its effect on the refractive indices control. Indeed, for the PP, when $\langle \Phi_{O_2} \rangle$ increases up to 0.4 sccm, n decreases linearly from 1.83 to 1.55, which is in agreement with the films' composition changing from N-rich to O-rich SiO_xN_y [32]. Then, for $\langle \Phi_{O_2} \rangle \geqslant 0.55$ sccm, the film's composition is stabilized close to an oxide one, and the refractive index slowly decreases from 1.5 to 1.45. Finally, the n range that is reached with the pulsed mode is the same than with the conventional mode (plotted as stars) between the nitride (2.03 at 1.95 eV [33]) and the oxide ones (1.46 at 1.95 eV [33]). In conclusion,

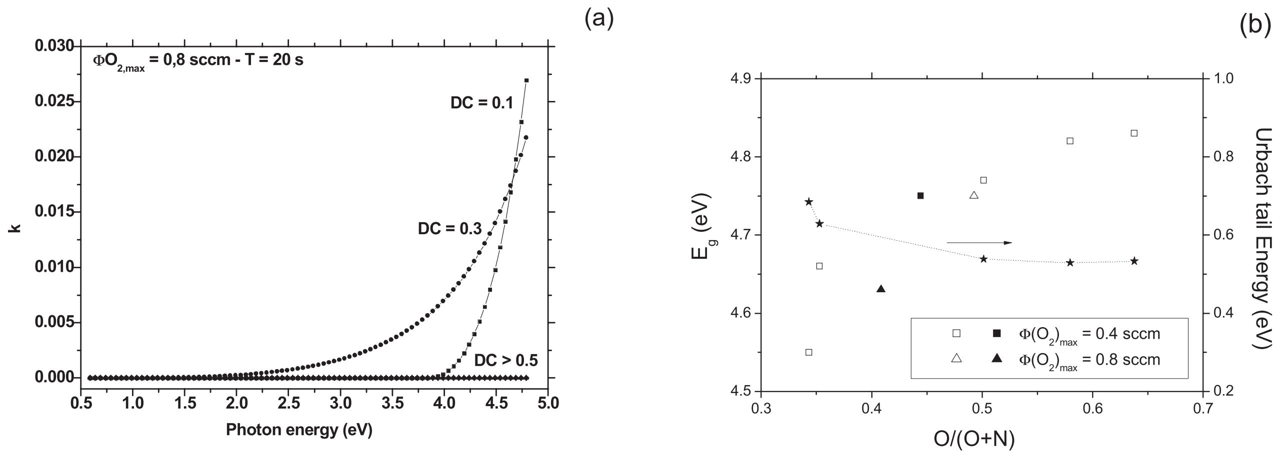

Figure 6. (a) Extinction coefficient as the function of photon energy for $\Phi_{max}(O_2) = 0.8$ sccm, $T = 20$ s and for various DC, and (b) the optical bandgap for various pulse conditions, $T = 20$ s (open) and $T = 40$ s (full), and Urbach tail energy for $\Phi_{max}(O_2) = 0.4$ sccm, $T = 20$ s.

by only changing the pulse parameters of one reactive gas, it is possible to tune the refractive index of the deposited material, which could be particularly interesting for optical devices such as multilayer ARCs.

However, before studying the antireflective multilayer optimized system, it is necessary to check the monolayer transparency. A first indication is given by the extinction coefficient k as a function of the wavelength, plotted in figure 6(a) for several pulse conditions. When the nitrogen content increases, while $\langle \Phi_{O_2} \rangle$ decreases, the extinction coefficient rises especially for the photon energy that is higher than 2.5 eV. However, even for the lowest DC, for the highest N-content film, k stays lower than 0.005 in the visible range (1.65–3.10 eV), and the films' IR and UV light absorption seems to be limited.

To confirm this, optical bandgaps are determined from UV–Visible spectroscopic measurements, considering an indirect gap in Tauc relationship [34], and they are plotted in figure 6(b). The optical bandgap increases from 4.55 to 4.83 eV when O/(O + N) content ratio increases from 0.34 to 0.64. For the higher O/(O + N) ratio, the optical bandgap can no more be determined from our measurements performed in the 1.1–6.0 eV range, meaning that values are higher than 5.0 eV. The referenced bandgaps for silicon nitride and oxide are respectively about 4.6 and 8.0 eV [33]. In our case, the values lower than 5.0 eV are consistent with oxynitride amorphous materials, as reported in [35]. In general, the optical absorption edge shape of amorphous films is directed by two phenomena: at high energy, absorption varies according to Tauc-type expression, whereas at low energy absorption, it follows an exponential function. This latter is due to a broadening of states because of a disordered structure besides the presence of the exponentially distributed states below the absorption edge. Indeed, the films defect level can be characterized by the exponential absorption edge's slope, called the Urbach tail energy, E_u, which is plotted in figure 6(b). For all films, E_u stays roughly between 0.7 and 0.5 eV, which is in agreement with values observed for amorphous oxynitride films [23, 36], taking into account that the values for O-rich films cannot be determined.

Finally, because of the large variation of refractive indices, in addition to the good transparency properties, we can use the SiO_xN_y films obtained with PP for antireflective multilayer systems.

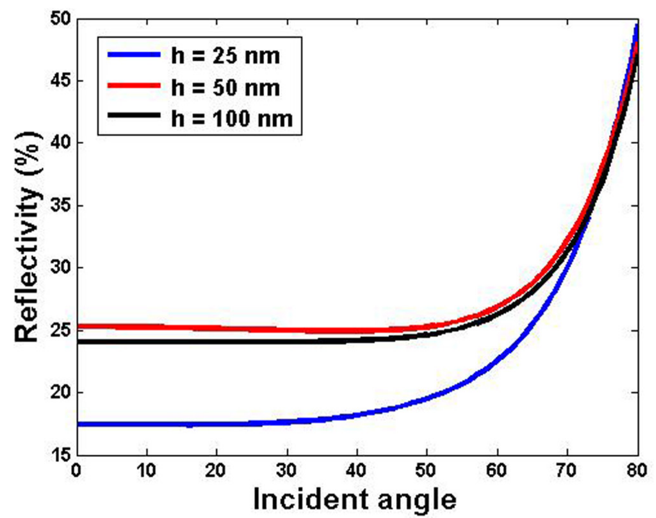

Figure 7. Simulated average reflectance as a function of the incident angle for various h.

3.4. Simulation and realization of antireflective system

The ARC was optimized by computing the reflectivity for a different number of layers. We found that the optimal structure is achieved with three layers presenting a linear spatial variation. In that case, the step refractive index function takes the following values (1.53, 1.66, 1.80) from the air-ARC interface to the Si-ARC interface. Furthermore, for the tri-layer ARC, the thickness of each layer was varied. In figure 7, the influence of the light incident angle on the ARC is studied. The averaged reflectivity over the wavelengths between 300 nm to 750 nm is then represented as a function of the incident angle for several individual thicknesses h. The lowest reflectivity (=18% for incident angle up to 45) is reached for an ARC of 75 nm total thickness, which corresponds to 25 nm per layer, and stays constant to the incident angle of 45°.

This optimal graded refractive index ARC was then deposited thanks to the RGPP technique and characterized.

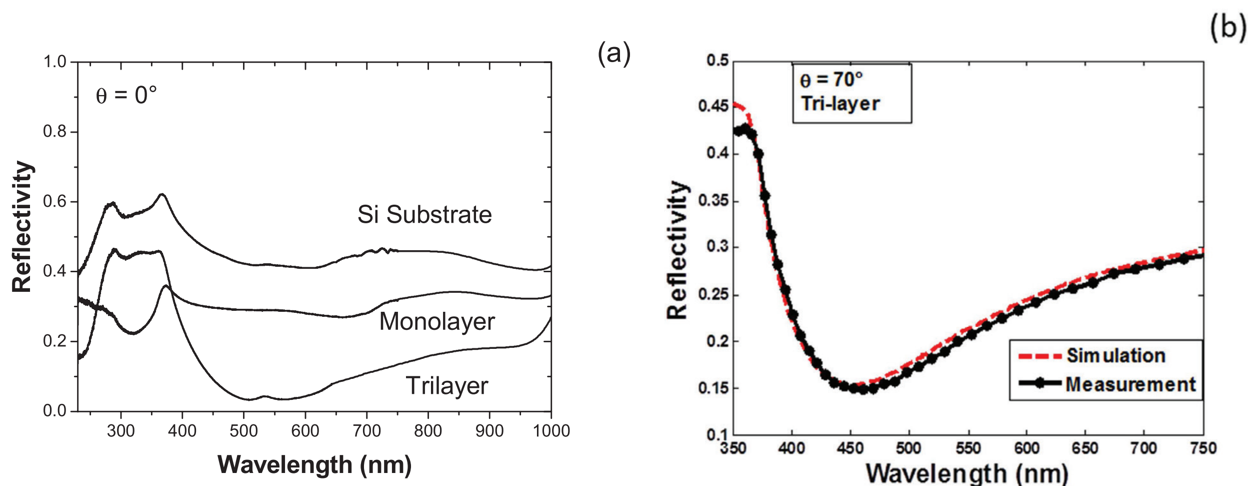

Figure 8. (a) The measured reflectivity for a normal incidence on a bare polished silicon substrate which is covered by optimized mono- and tri-layer ARC, and (b) the measured and simulated reflectivity for a 70° incident angle.

The measured reflectivity for a normal incidence is represented in figure 8(a) for a bare polished Si substrate taken as a reference, and this is then covered with an AR system: either a monolayer, which is expected to be the first layer (25 nm, $n = 1.8$) of the tri-layer ARC system, or the optimized tri-layer. We might notice that the monolayer allows a decrease of the silicon reflectivity by a third, whereas as predicted with the model calculations, low reflectivity values are reached with the tri-layer. This trilayer presents a minimum reflectivity of 3.0% around 510 and 520 nm and an averaged reflectivity in the visible range (400–750 nm range) of 8.1%. This result is comparable to the one obtained in the literature for the same refractive index range and without substrate texturation [37, 38].

In addition, in order to check the refractive index and the thickness of each real layer in the tri-layer system, we performed a comparison between the experimental and theoretical reflectivity spectra. To do so, we studied the tri-layer system by ellipsometry at 70° (as the only available incident angle with this apparatus) and fit the experimental data. An almost perfect agreement is achieved for thicknesses (25, 34.5, 30) nm, which corresponds to the respective refraction index variation (1.53, 1.66, 1.80) and is presented on figure 8(b). The small discrepancy is due to a difference either in thicknesses or refractive indices between the model results and the realized structure. This could be explained by a slight variation in the estimated deposition rate for very thin films. But, we think that this difference is more likely linked to a small difference in refractive indices. Indeed, the optimized refractive indices, as mentioned previously, are (1.53, 1.66, 1.80) from the air-ARC interface to the Si-ARC interface, whereas the refractive indices of realized films are (1.55, 1.66, 1.80). This small difference of the upper layer refractive index could be the reason of such a small observed difference.

Finally, this optimized ARC system is realized easily and quickly thanks to the RGPP technique. Hence, with the deposition rates higher than 20 nm min^{-1} obtained with this process, the tri-layer system is deposited in less than 4 min.

4. Conclusion

In this paper, the RGPP is used as a powerful technique to control finely the composition of the SiO_xN_y films and then the refractive indexes, only by tuning the pulsing conditions. We demonstrate that a large range of refractive indices can be reached, in comparison to the one reached in CP, without drastically reducing the deposition rate. Furthermore, it is possible to go forward and use it to obtain the antireflective multilayer system. For this goal, an ARC structure is optimized using a genetic algorithm and then realized with the RGPP technique. A reflectivity reduction by a factor of six is observed compared to bared polished silicon wafer, reaching the averaged reflectivity lower than 8.1% (in 400–750 nm visible light range). Nevertheless, this reflectivity result could further be improved. If we go forward, a more efficient graded refractive index system could be reached by enlarging the refractive index window which matches the silicon and the air indices. Furthermore, we could imagine that, in addition to the interferential effect, the contribution of the graded structure on the reflectivity.

Acknowledgments

This work was founded by the French National Research Agency, the European Commission (Feder funds) and the Région Auvergne in the Framework of the LabEx IMobS[3].

References

[1] Bedjaoui M and Despax B 2010 Physico-chemical, structural and physical properties of hydrogenated silicon oxinitride films elaborated by pulsed radiofrequency discharge *Thin Solid Films* **518** 4142–9

[2] Martin N, Sanjines R, Takadoum J and Levy F 2001 Enhanced sputtering of titanium oxide, nitride and oxynitride thin films by the reactive gas pulsing technique *Surf. Coat. Technol.* **142–4** 615–20

[3] Cristea D, Constantin D, Crisan A, Abreu C S, Gomez J R, Barrada N P L, Alves E, Moura C, Vaz F and Cunha L 2013 Properties of tantalum oxynitride thin films produced by magnetron sputtering: the influence of processing parameters *Vacuum* **98** 63–9
[4] El-Oyoun H, Inokuma T, Kurata Y and Hasegawa S 2003 *Japan. Appl. Phys.* **42** 3570
[5] Hoffmann P, Smeisser D, Beck R B, Cuch M, Giedz M and Jakubowski A 2004 *J. Alloys Compd.* **382** 228–33
[6] Iwamori S, Gotoh Y and Moorthi K 2002 *Vacuum* **68** 113–7
[7] Shim J, Yoon H G, Na S H, Kim I and Kwak S 2008 *Surf. Coat. Technol.* **202** 2844–9
[8] Hallam B, Tjahjono B and Wenham S 2012 *Sol. Energy Mater. Sol. Cells* **96** 173–9
[9] Laades A, Bukhardt M, Roczen M, Klimm C, Blech M and Lawerenz A 2012 *Phys. Status Solidi* c **9** 2124–7
[10] Brinkmann N, Sommer D, Micard G, Hahn G and Terheiden B 2013 *Sol. Energy Mater. Sol. Cells* **108** 180–8
[11] Lipiński M, Kaminski A, Lelièvre J-F, Lemiti M, Fourmond E and Zięba P 2007 *Phys. Status Solidi c* **4** 1566–9
[12] Rebib F, Tomasella E, Dubois M, Cellier J, Sauvage T and Jacquet M 2007 *Thin Solid Films* **515** 3480–7
[13] Nakanishi Y, Kato K, Omoto H and Takamatsu A 2012 *Thin Solid Films* **520** 3862–4
[14] Berg S and Nyberg T 2005 *Thin Solid Films* **476** 215–30
[15] Barankova H, Berg S, Carlsson P and Nender C 1995 *Thin Solid Films* **260** 181–6
[16] Bousquet A, Zoubian F, Cellier J, Sauvage T and Tomasella E 2013 *Plasma Process. Polym.* **10** 990–8
[17] Sproul W D, Christie D J and Carter D C 2005 *Thin Solid Films* **491** 1–17
[18] Aronson A J, Chen D and Class W H 1980 *Thin Solid Films* **72** 535
[19] Petitjean C, Grafouté M, Rousselot C and Pierson J F 2008 *Surf. Coat. Technol.* **202** 4825–9
[20] Aubry E, Weber S, Billard A and Martin N 2011 *Appl. Surf. Sci.* **257** 10065–71
[21] Aubry E, Weber S, Billard A, Martin N 2014 *Appl. Surf. Sci.* **290** 148–53
[22] Chattopadhyay S, Huang Y F, Jen Y J, Ganguly A, Chen K H and Chen L C 2010 *Mater. Sci. Eng.* **R69** 1–35
[23] Layer M 1997 *SMINRA User's Guide* (*Report IPP*) vol 9/113 (Germany: Max-Planck-Institut Fur Plasmaphysik)
[24] Forouhi A R and Bloomer I 1986 *Phys. Rev.* B **34** 7018–26
[25] Forouhi A R and Bloomer I 1988 *Phys. Rev.* B **38** 1865
[26] Jellison G E and Modine F A 1996 *Appl. Phys. Lett.* **69** 371–4
[27] Southwell W H 1983 *Opt. Lett.* **8** 584–6
[28] Defrance J *et al* 2016 *J. Open Res. Softw.* **4** 13
[29] Taviot-Guého C, Cellier J, Bousquet A and Tomasella E 2015 *J. Phys. Chem.* C **119** 23559–71
[30] He L, Inokuma T, Kurata Y and Hasegawa S 1995 *J. Non-Cryst. Sol.* **185** 249
[31] Savall C, Bruyère J C and Stoquert J P 1995 *Thin Solid Films* **260** 174
[32] Wong H 2002 *Microelectron. Reliab* **42** 317–26
[33] Palik E D 1985 *Handbook of Optical Constants of Solid* (New York: Academic) p 760, 774
[34] Tauc J, Grigonovici R and Vancu A 1966 *Phys. Status Solidi* **15** 627
[35] Rebib F, Tomasella E, Micheli V, Eypert C, Cellier J and Laidani N 2009 *Opt. Mater.* **31** 510–3
[36] Signore M A, Sytchlova A, Dimaio D, Cappello A and Rizzo A 2012 *Opt. Mater.* **34** 632–8
[37] Lee Y Y, Ho W J and Yeh C W 2015 *Appl. Surf. Sci.* **354** 20–4
[38] Kuo T W, Wang N F, Tsai Y Z, Hung P K and Houng M-P 2014 *Mater. Sci. Semicond. Process.* **25** 211–8